Office of Naval Research

Contract N00014-67-A-0103-0018

NR 064 478

Technical Report No. 13

CRACK BRANCHING IN HOMALITE-100 SHEETS

by

A. S. Kobayashi, B. G. Wade, W. B. Bradley and S. T. Chiu

June 1972

The research reported in this technical report was made possible through support extended to the Department of Mechanical Engineering, University of Washington, by the Office of Naval Research under Contract N00014-67-A-0103-0018, NR 064 478. Reproduction in whole or in part is permitted for any purpose of the United States Government.

Department of Mechanical Engineering
College of Engineering
University of Washington

Security Classification

DOCUMENT CONTROL DATA - R & D

(Security classification of title, body of abstract and indexing annotation must be entered when the overall report is classified)

1 ORIGINATING ACTIVITY *(Corporate author)* Department of Mechanical Engineering University of Washington Seattle, Washington 98195	2a. REPORT SECURITY CLASSIFICATION Unclassified 2b. GROUP

3 REPORT TITLE

"Crack Branching in Homalite-100 Sheets"

4 DESCRIPTIVE NOTES *(Type of report and inclusive dates)*

Interim Report

5 AUTHOR(S) *(First name, middle initial, last name)*

A. S. Kobayashi, B. G. Wade, W. B. Bradley and S. T. Chiu

6 REPORT DATE	7a. TOTAL NO. OF PAGES	7b. NO OF REFS
June, 1972	27	14

8a CONTRACT OR GRANT NO	9a. ORIGINATOR'S REPORT NUMBER(S)
N00014-67-A-0103-0018 b. PROJECT NO NR 064 478 c. d.	9b. OTHER REPORT NO(S) *(Any other numbers that may be assigned this report)*

10 DISTRIBUTION STATEMENT

Unlimited

11 SUPPLEMENTARY NOTES	12. SPONSORING MILITARY ACTIVITY
	Office of Naval Research

13 ABSTRACT

Crack branching in Homalite-100 sheets of 1/8-inch and 3/8-inch thickness was studied by using dynamic photoelasticity. Dynamic stress intensity factors, crack velocities and branching angles were measured. Corresponding static stress intensity factors were determined by the method of finite element analysis. Dynamic stress intensity factors reached a peak value at branching with a value of three times larger than the fracture toughness of the material and preceded the actual branching. The dynamic stress intensity factor after branching drops and then increases again to the maximum stress intensity at which point branching occurs again. Roughness of the fracture surface can be related to a dynamic stress intensity factor and crack velocities near the branching stress intensity factors and terminal crack velocities, respectively. Average branching angle was 26 degrees.

Details of illustrations in this document may be better studied on microfiche

DD FORM 1 NOV 65 1473 (PAGE 1)

0102-014-6600

Security Classification

14 KEY WORDS	LINK A		LINK B		LINK C	
	ROLE	WT	ROLE	WT	ROLE	WT
Fracture mechanics						
Crack propagation						
Crack Branching						
Finite Element Analysis						
Dynamic Photoelasticity						

11

CRACK BRANCHING IN HOMALITE-100 SHEETS

by

A. S. Kobayashi, B. G. Wade, W. B. Bradley and S. T. Chiu

ABSTRACT

Crack branching in Homalite-100 sheets of 1/8-inch and 3/8-inch thickness was studied by using dynamic photoelasticity. Dynamic stress intensity factors, crack velocities and branching angles were measured. Corresponding static stress intensity factors were determined by the method of finite element analysis. Dynamic stress intensity factors reached a peak value at branching with a value of three times larger than the fracture toughness of the material and preceded the actual branching. The dynamic stress intensity factor after branching drops and then increases again to the maximum stress intensity at which point branching occurs again. Roughness of the fracture surface can be related to a dynamic stress intensity factor and crack velocities near the branching stress intensity factors and terminal crack velocities, respectively. Average branching angle was 26 degrees.

CRACK BRANCHING IN HOMALITE-100 SHEETS

by

A. S. Kobayashi, B. G. Wade, W. B. Bradley and S. T. Chiu

INTRODUCTION

When a running crack in a brittle material reaches a terminal velocity, the crack normally branches, momentarily decelerates, and then accelerates to a terminal velocity where it will branch again. In highly loaded brittle materials this process is repeated many times thus resulting in fragmentation of the material.

Branching cracks in glass have been studied by Schardin through the use of high-speed photography with a spark-gap camera (1, 2)*. More recently Clark and Irwin (3) and Sih and Irwin (4) have discussed the dynamic unloading effects and the influence of crack speed on the crack opening displacements. In Reference 4 the dynamic stress concentration of a circular hole expanding at a constant velocity was used to estimate a dynamic correction factor to Westmann's static solution (5) of a pressurized star-shaped crack in order to obtain the strain energy release rate of a multiple branching crack. For a crack velocity one-half of the Rayleigh wave velocity, the strain energy release rate was then estimated to be approximately 23 percent above its static values.

Since elastodynamic solutions of an accelerating or a decelerating crack as well as that of a constant velocity branching crack are not in sight, it appears that only experimental analysis can provide information on the intriguing problem of crack branching at this time. In the course of four

---

*Numbers in parenthesis refer to references at the end of this paper.

years of investigation on dynamic crack behaviors, we have inadvertently accumulated sufficient data on crack branching and thus an analysis of this phenomena became feasible. An account of our findings on crack branching by the use of dynamic photoelasticity and some comparison with static results obtained by finite element analysis are given in the following.

EXPERIMENTAL PROCEDURE AND RESULTS

The modified Cranz-Schardin 16 spark-gap camera and associated dynamic polariscope used in this investigation were described in previous papers (6,7,8). The test specimens considered in these series of tests consisted of 3/8-inch and 1/8-inch thick Homalite-100 plates with 10 x 10 inch test section loaded in fixed grip configuration. The prescribed boundary conditions included both uniform and linearly decreasing displacements along the fixed gripped edges of the specimen. At fracture load, the crack propagated from a single, edge-notched starter crack which was saw cut and chiseled. This crack, as shown in Figures 1-6, normally branched several times before propagating through the plate. In the 3/8-inch thick specimens, many nonpropagating branch cracks such as those prominently shown in Figure 4 were formed. Such minute branch cracks were not detected in the 1/8-inch thick specimens shown in Figures 1, 2 and 6. Figure 6 shows branch cracks in a tension plate with a hole. The hole with its localized region of static stress concentration did not have significant influence on the path of the running crack despite the inner connected isochromatics shown in Frames 10 and 11. This branch crack thus missed the hole and continued through the plate.

Most of the Homalite-100 sheets used in these experiments were calibrated by Bradley (6) who reported an average dynamic modulus of elasticity,

Poisson ratio, stress-optic coefficient, and static fracture toughness of 675 ksi, 0.345, 155 psi-in/fringe, and 579 psi $\sqrt{in.}$ respectively. The calibration data obtained for the 3/8-inch thick sheets were also used to estimate the material and optical properties of the 1/8-inch thick sheets used in Specimen Numbers 1, 2, 6 and 7.

Table 1 summarizes the experimental results of seven specimens which exhibited prominent crack branching. Included angles of crack branching were measured for all major branches. The average included angle of 26° for branch cracks is approximately half of the 60° predicted by Yoffe (9). These experimental results are in agreement with Clark's and Irwin's observation in Reference 3.

DYNAMIC STRESS INTENSITY FACTOR

Dynamic stress intensity factors were determined from the dynamic photoelasticity patterns using Bradley's approximate procedure (6) which is a variation of the original procedure suggested by Irwin (10). Bradley assumed that the unknown remote stress component, σ_{0x}, is equal to the applied stress of σ and then reduced Irwin's two parameter representation of the near-field isochromatics to a one parameter representation. Such one parameter representation, when used in Irwin's formulation (10) of stress intensity factor versus isochromatics could introduce significant errors in computing stress intensity factors. An assessment on such possible error involved due to the use of a wrong remote stress, σ_{0x}, has been discussed in detail by C. W. Smith (11,12) where errors as much as 20% are reported.

In order to reduce the sensitivity of stress intensity factor determination to the remote stress Bradley then computed, with the assumption of $\sigma = \sigma_{0x}$, the stress intensity factor by utilizing data from two adjacent

isochromatics, τ_1 and τ_2, located at radial distances of r_1 and r_2 from the crack tip respectively (6). Although the advantage of this technique over the original procedure by Irwin (10) was demonstrated, no quantitative assessment was made on the influence of the assumption of $\sigma = \sigma_{0x}$. Following the paper of C. W. Smith (12), an estimate of this influence was made by setting $\sigma_{0x} = \delta \cdot \sigma$. Bradley's expression for stress intensity factor is then changed to:

$$K_I = 2\sqrt{2\pi}\,(\tau_2 - \tau_1)\left[\frac{\sqrt{r_1 r_2}}{f_2\sqrt{r_1} - f_1\sqrt{r_2}}\right] \qquad (1)$$

where

$$f_i\,(\theta, r_i, a) = \left[\sin^2\theta + \delta\,\frac{2\sqrt{2r_i}}{\sqrt{a}}\sin\theta\sin\frac{3\theta}{2} + \frac{2\delta^2 r_i}{a}\right]^{1/2} \qquad i = 1 \text{ or } 2$$

a is the crack length of the edge notched specimen

θ is the angular orientation of polar coordinate (r_i, θ) with origin at the crack tip

$\delta = 1$ in Equation 1 coincides with Bradley's expression (6). The stress intensity factors for a range of $\delta = -1.0$ to 2.0 were then computed for Test No. 3 shown in Figure 7. The scatter band due to this variation in δ was not larger than the size of the data points in Figure 7. As shown by this example, Bradley's approximate procedure appears insensitive to the exact value of the remote stress, σ_{0x}, and thus provides reasonably accurate one-parameter procedure of determining stress intensity factors from the near-field isochromatics.

The procedure described above is not useful in evaluating the dynamic stress intensity factor of closely spaced branching cracks such as those shown in Figures 4 and 5. The lack of distinct butterfly-shaped isochromatic loops adjacent to the crack tip makes it impractical to use either Irwin's or Bradley's approaches. This difficulty could be removed by increased

optical resolution which would provide higher order isochromatic loops in the immediate vicinity of the crack tip. The local dimpling in the vicinity of the crack tip, however, places practical limitation on the optical resolution which cannot be improved by conventional techniques. For example, the conventional immersion technique will not work under the dynamic loading since cavitation at the specimen-fluid interface will obscure all isochromatic fringes gained by such immersion.

A different procedure was thus developed to evaluate the dynamic photoelastic patterns of a branching crack. The near-field static isochromatics of closely-spaced, parallel cracks were considered same as to the dynamic isochromatics near the crack tips of multiple branched long cracks. As for the static solution, available analytical solutions (13, 14) did not match the boundary conditions represented by this idealized problem nor were the crack spacings close enough and thus these solutions could not be used.

As a result, a finite element analysis was made on an edge-cracked plate of unit width and with a prescribed edge displacement of unity. The legend of Figure 8 shows the plate configuration used for the finite element analysis, which included a typical nodal breakdown of 400 elements and 451 nodal points. The static stress intensity factor was obtained by computing the strain energy release rate in a manner described in Reference 8.

A comparison between the above static finite element analysis and dynamic isochromatics is shown in terms of physical dimensions in Figure 8. The dynamic isochromatic pattern which was considered, lies between the first and second right branch cracks in Frame No. 12 of Test No. 5. The physical dimensions of the finite element model was scaled by a factor of $\sqrt{b}$ where b is the half distance between the first and second branch cracks. The computed maximum isochromatics from the finite element analysis was scaled by varying

the applied edge displacements until it matched the experimental isochromatics along the edge boundary. The stress intensity factor of the original finite element analysis was then compensated by applying the above geometric and load scaling factors. The resultant stress intensity facotr of the right branch crack shown in Frame 12 of Test No. 5 is 1223 psi$\sqrt{in.}$

The left side of this particular branch shows distinct isochromatic loops due to lack of a closely spaced branch crack on the left side. This isochromatic pattern was analyzed by the Bradley procedure which yielded a stress intensity factor of 1261 psi$\sqrt{in.}$. Thus good agreement was obtained between the stress intensity factor determined by Bradley's procedure and the closely spaced parallel crack solution for the same branch crack.

The above static solution of closely spaced parallel cracks were used together with Bradley's procedure to evaluate the dynamic stress intensity factors of Tests 2, 3, 5 and 7. Test No. 4 was omitted from evaluation due to the abundance of short, multiple, and non-propagating branch cracks, shown prominently in Figure 4. These multiple branch cracks obscurred the near field isochromatics and could not be analyzed readily. Presumably, a finite element analysis could be conducted to obtain a corresponding static solution which could then be used in a procedure similar to the multiple branched cracks described previously. Test No. 6 did not yield regularly sequenced dynamic photoelastic pictures due to malfunction in the timing circuitry and therefore was not evaluated.

EVALUATION OF DATA

Figures 7a and 7b show the dynamic stress intensity factors and crack velocities of the two main branch cracks shown in Figure 3. Also shown is the static

stress intensity factor determined by the method of finite element analysis for a symmetrically branched crack with edge displacements of Test No. 3 prescribed. This specific finite element analysis involved 606 elements and 656 nodal points with the crack tip element dimensions of 2.5×10^{-2} in. The static stress intensity factor was obtained by comparing the values of total strain energy of two cracked plates with slightly different crack lengths. The Mode II stress intensity factors were computed using the values of crack opening displacements of the crack surface. Figure 9 shows this static stress intensity factor in dimensionalized and non-dimensionalized form as well as the corresponding static stress intensity factor for single crack (8). Also shown in Figure 9 is the Mode II stress intensity factor, K_{II}, which, although small, exists in this slant mode of crack propagation after branching. Figure 10 shows fractured surfaces of the left and right branch cracks of this test. Considerable surface roughness is observed in the right branch crack after branching while the left branch crack shows a smooth surface after branching.

Figure 11 shows the dynamic stress intensity factors and crack velocities of the left and right major branch cracks for Test No. 5 shown in Figure 5. Static stress intensity factors, although not impossible to compute, were not obtained by the method of finite element analysis. Figure 12 shows the fracture surfaces of these two major branch cracks. Again considerable surface roughness was observed on both branch cracks after the first branching.

Figures 13 and 14 show the crack velocities of left and right branch cracks for Test Nos. 1 and 2 which involves a 1/8 inch thick plate shown in Figures 1 and 2. The lack of higher order isochromatic loops at the crack tip of Test No. 2 made it impractical to evaluate the dynamic stress intensity factors of this test. Static stress intensity factors for the two were obtained by superposing the finite element solution described previously and a separate finite element solution for a

plate with linearly decreasing edge displacements. Since the location of the first crack branching in Test No. 2 differed with that of Figure 8, and of Test No. 2 and 3, an appropriate shifting of the stress intensity factor was necessary in order to obtain the static results. The resultant static results in Figure 14 should thus be considered as an estimate for reference purpose only.

Figure 15 shows the dynamic stress intensity factors and crack velocities for the two major branches in Test No. 7 which again involves a 1/8 inch thick plate. The corresponding static stress intensity factors for this test was not attempted due to the complexity of the crack geometries. The rather high dynamic stress intensity factor observed in the left branch could be due to experimental errors due to the lack of optical sensitivity of the 1/8 inch plate as well as the lack of accurate calibration data on the stress-optic law of this plate.

DISCUSSION

The dynamic stress intensity factors determined by dynamic photoelasticity show that there exists a branching stress intensity which is approximately 1800 psi$\sqrt{\text{in.}}$ and 2200 psi$\sqrt{\text{in.}}$ for the 3/8 inch and 1/8 inch thick Homalite 100 plates, respectively. This branching stress intensity factor is approximately 3 4 times larger than the static fracture toughness of the material.

Although not conclusive, the branching stress intensity factor is reached prior to branching and hence prior to the corresponding static branching stress intensity factor as shown in Figures 8 and 13. This conclusion is in agreement with Bradley's conclusion that the change in dynamic stress intensity factor preceeds the change in crack velocity, which in this branching problem corresponds to the location of crack branching (6, 7).

As expected, the crack velocity drops to a minimum value at branching and then reaccelerates to higher value for another branching. The fluctuating velocities

and the minimum values in Figures 11 and 14, for example, can be related to locations of crack branches.

The surface roughness shown in Figures 10 and 12 can be correlated directly with the crack velocity of approximately 14,000 inch/sec and above in 3/8 inch thick plates. Little surface roughness is observed in the 1/8 inch plate although crack velocities in excess of 14,000 inch/sec were observed in all tests. Perhaps this difference could be attributed to differences in the plane strain versus plane stress states due to the change in thickness.

Finally as an interesting sideline, Figure 16 shows an enlarged view of Frame No. 11 of Test No. 5 where an isochromatic pattern of Mode II crack deformation is shown at the crack top of the extreme left branch. The crack tip stress intensity factor of this branch expressed in a manner similar to Equation 1 is:

$$K_{II} = 2\sqrt{2\pi}\,(\tau_2 - \tau_1)\,\sqrt{\frac{r_1 r_2}{r_1 - r_2}}\;\Big/\;\sqrt{3\sin^2\theta + 1} \qquad (2)$$

This Mode II stress intensity factors varied from 210 to 154 psi$\sqrt{\text{in.}}$ in Frames 11 - 12 of Test No. 5. A check of Test No. 4 shows that a multiple of Mode II crack tip deformations are shown by this typical isochromatic pattern. It appears that an arrested crack left behind the bulk of an advancing crack can be identified with this Mode II crack deformation pattern.

ACKNOWLEDGEMENT

This research project was sponsored by the Office of Naval Research Contract No. N00014-67 0103-0018 NR 064 478. The writers wish to [illegible] Mr. J. H. Crowley and Dr. N. Perrone of ONR for their patience and encouragement during the course of this investigation.

ASK/mw 6/6/72

REFERENCES

1. H. Schardin, D. Elle, and W. Struth, "Uber den zeitllchen Ablauf des Bruchvorganges in Glas und Kungstglas," Zeit. Tech. Physik, 21, 1940, pp. 393.

2. H. Schardin, "Velocity Effiects in Fracture, " Fracture (edited by B. L. Averbach), Wiley, 1959, pp. 297-330.

3. A. B. J. Clark and G. R. Irwin, "Crack Propagation Behavior," Experimental Mechanics, 6, No. 6, June 1969, pp. 321-30.

4. G. C. Sih and G. R. Irwin, "Dynamic Analysis for Two Dimensional Multiple Crack Division," Engineering Fracture Mechanics, 1 April 1970, pp. 603-614.

5. R. A. Westmann, "Pressurized Star Crack," J. of Math. Phys. and Solids, 69, 1964, pp. 191-198.

6. W. B. Bradley and A. S. Kobayashi, "An Investigation of Propagating Cracks by Dynamic Photoelasticity," Experimental Mechanics, Vol. 10, No. 3, March 1970, pp. 106-113.

7. W. B. Bradley and A. S. Kobayashi, "Fracture Dynamics--A Photoelastic Investigation," Engineering Fracture Mechanics, Vol. 3, 1971, pp. 317-332.

8. A. S. Kobayashi, B. G. Wade, and D. E. Maiden, "Photoelastic Investigation on the Crack-Arrest Capability of a Hole," Experimental Mechanics, Vol. 12, Jan., 1972, pp. 32-37.

9. E. H. Yoffe, "The Moving Griffith Crack," Phil. Mag., Vol. 42, 1951, pp. 739-750.

10. G. R. Irwin, Discussion and Authors' Closure of the Paper, " The Dynamic Stress Distribution Surrounding a Running Crack--A Photoelastic Analysis," Proc. of SESA, Vol. XVI, No. 1, 1958, pp. 93-96.

11. G. R. Marrs and C. W. Smith, "A Study of Local Stresses Near Surface Flaws in Bending Fields," to be published in ASTM STP 513.

12. M. A. Schroedl, J. J. McGowan, and C. W. Smith, "An Assessment of Factors Influencing Data Obtained by the Photoelastic Stress Freezing Technique for Stress Fields Near Crack Tips," to be published in the J. of Engineering Fracture Mechanics.

13. W. B. Ficher, "Stresses at the Tip of a Longitudinal Crack in a Plate Strip," NASA, TR R-265, August 1967.

14. K. Watanabe and A. Atsuru, "Infinite Row of Parallel Cracks in a Strip," International Journal of Engineering Sciences, Vol. 10, 1972, pp. 173-184.

ASK/mw 6/7/72

Test No.	Plate Thickness (in.)	Loading ε top	Loading ε bottom	(in/in)	Terminal Crack Velocity (in/sec)	Included Branch Angle No. 1	No. 2	No. 3	No. 4	No. 5	No. 6	No. 7	No. 8	No. 9
1	1/8	0.00172	0.00165		14,000	23°	23°	23°	31°*	29°*				
2	1/8	0.00206	0.000366		15,700	30°*	31°*	31°*						
3	3/8	0.00153	0.00156		15,300	30°*	20°*	14°*	28°	19°				
4	3/8	0.00914	01000870		15,400	30°*	29°*	21°*	22°*	21°*	25°	14°*	19°*	30°*
5	3/8	0.00325	0.00325		15,200	28°*	19°	26°*	17°*	23°*	19°	31°*	34°	34°
6	1/8					30°*	32°*	30°*	25°	25°				
7	1/8				16,200	32°*	28°*							
Average Branch Angle						29°	26°	24°	25°	23°	22°	23°	27°	32°

Average of all Branch Angles - 26°

* Asterisk indicated a main crack front. Others w/o asterisk indicate a secondary side branch of short length which were arrested.

TABLE I SUMMARY OF EXPERIMENTAL RESULTS

ASK/mw 6/7/72

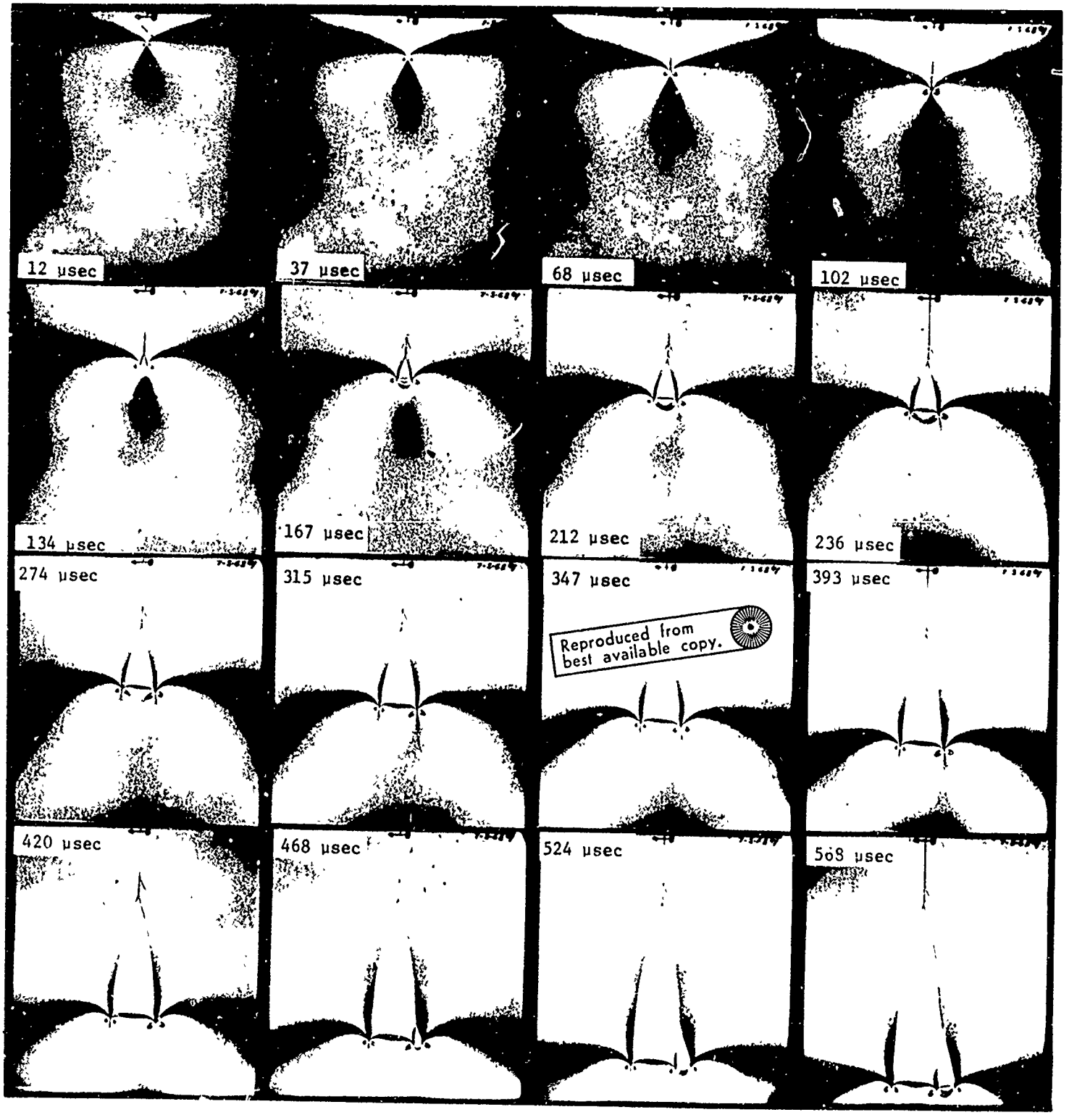

Figure 1. Isochromatic Patterns of Dynamic Crack Propagation for Test No. 1

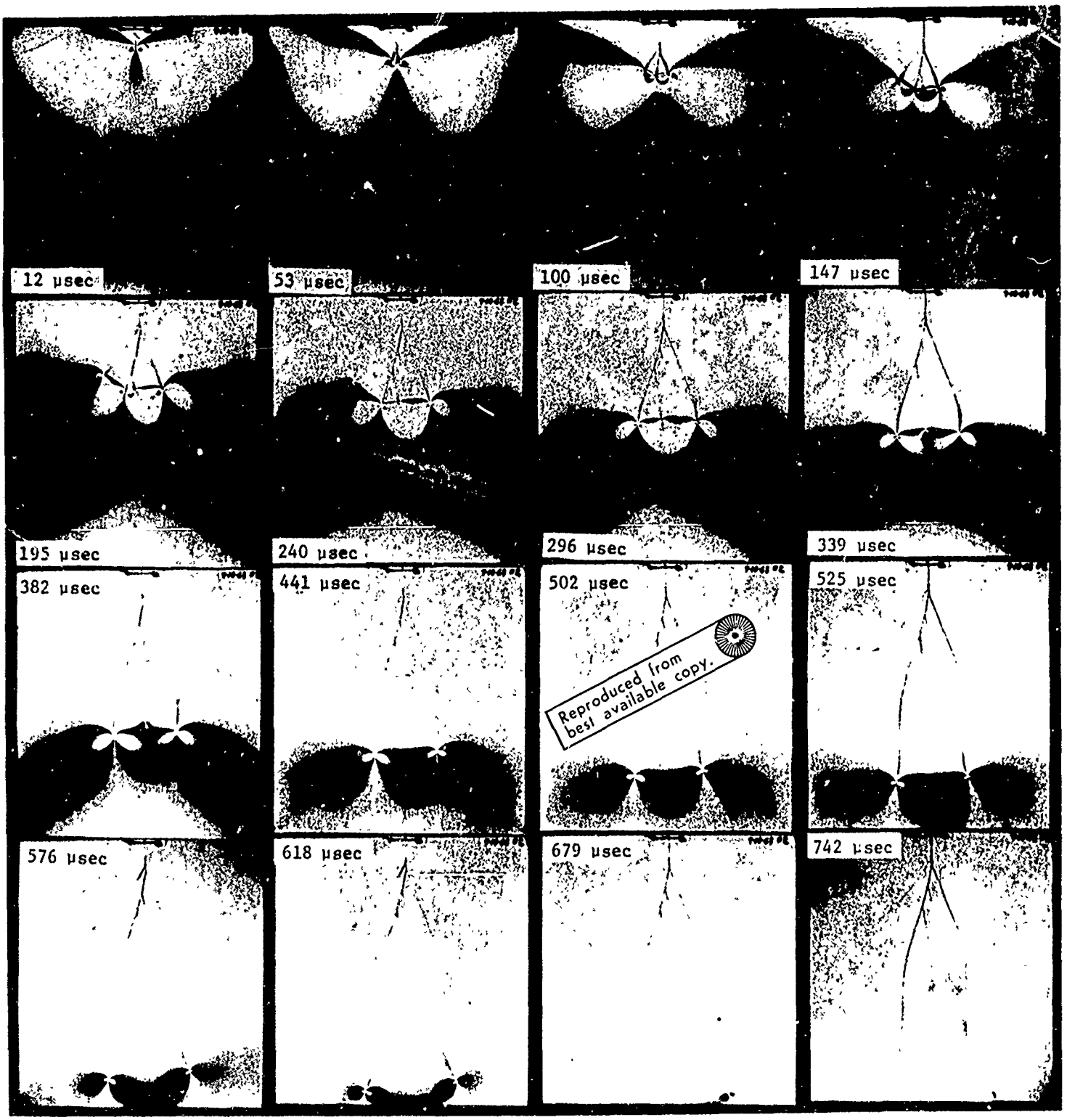

Figure 2. Isochromatic Patterns of Dynamic Crack Propagation for Test No. 2

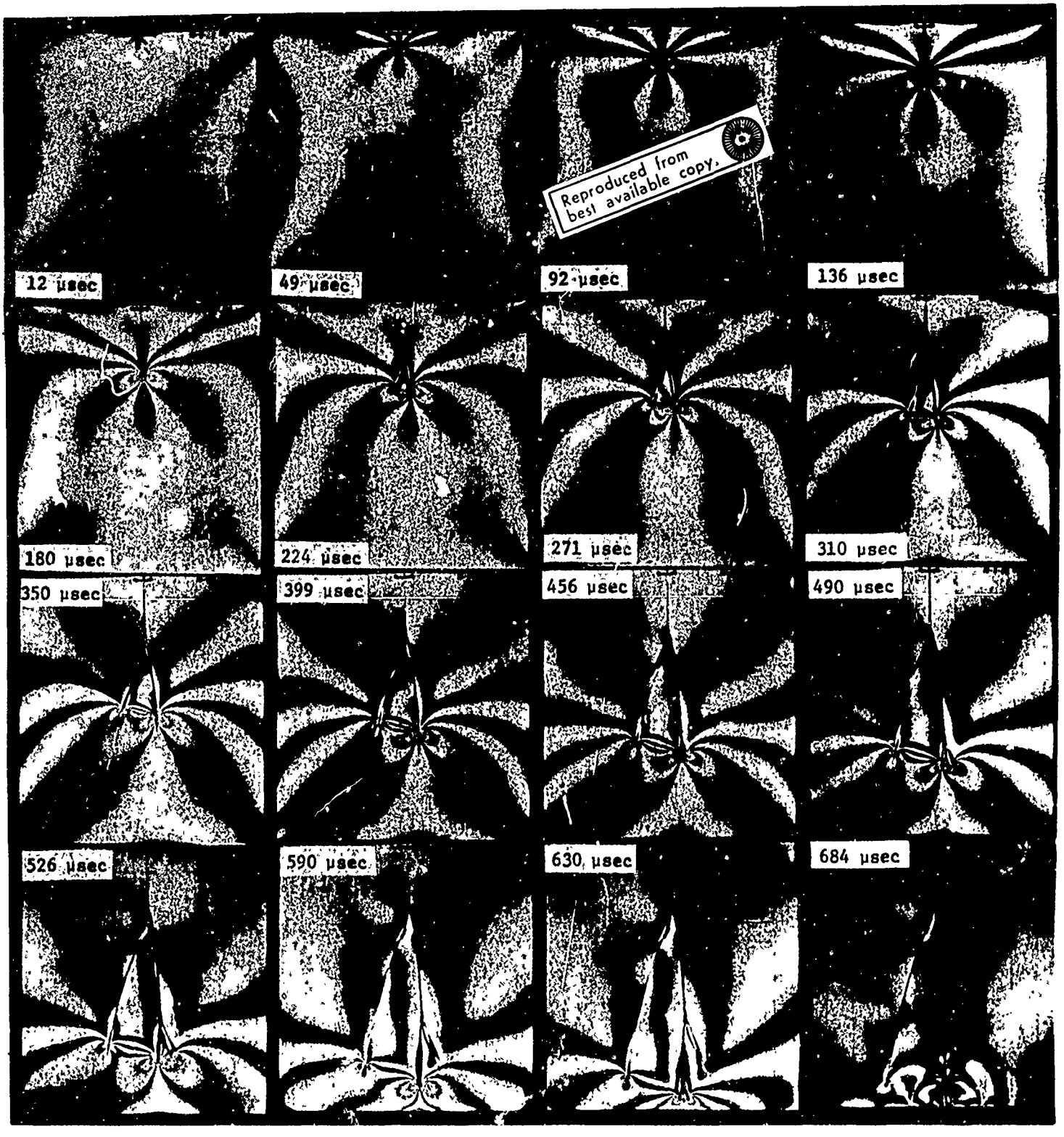

Figure 3. Isochromatic Patterns of Dynamic Crack Propagation for Test No. 3

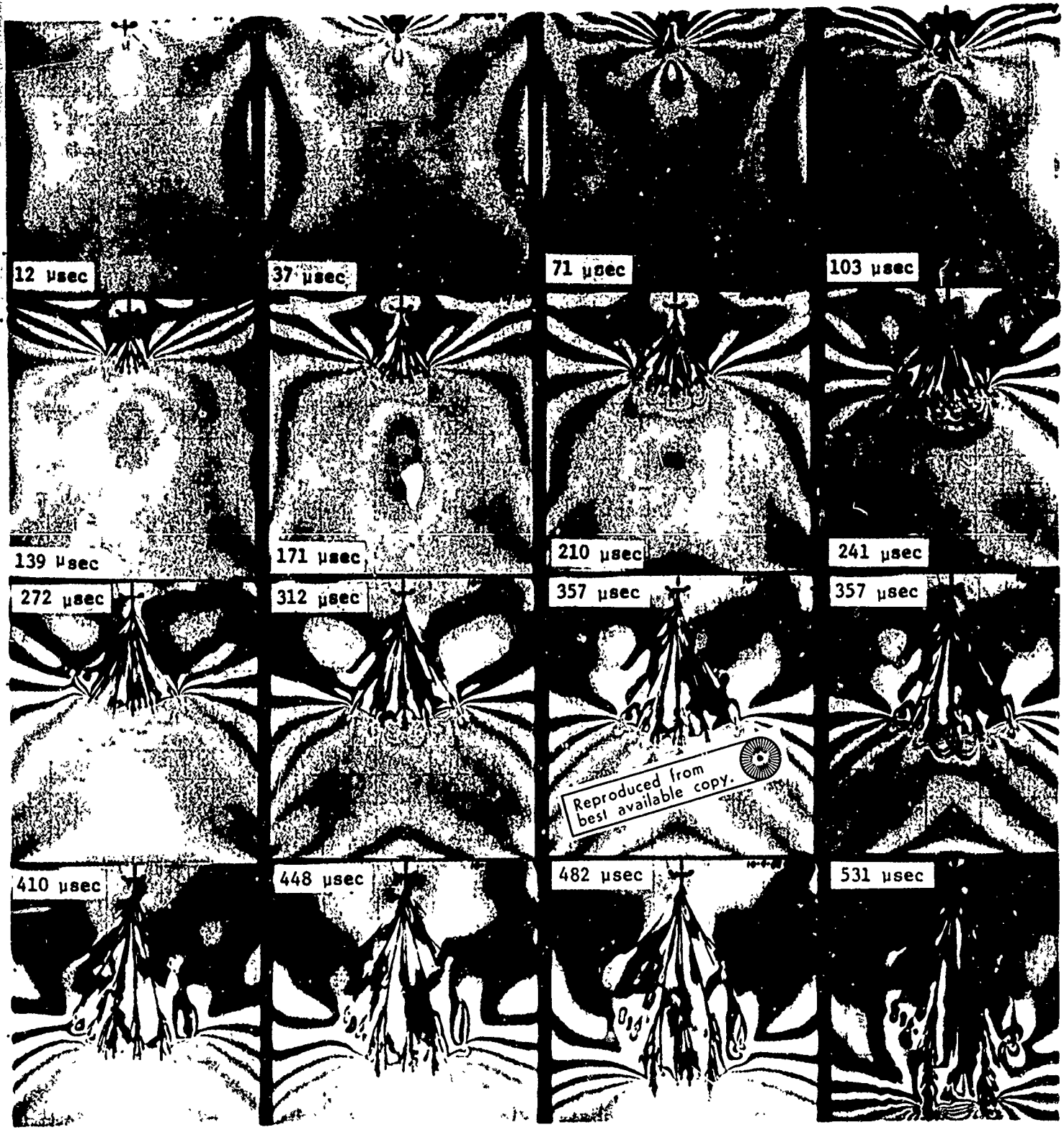

Figure 4. Isochromatic Patterns of Dynamic Crack Propagation for Test No. 4

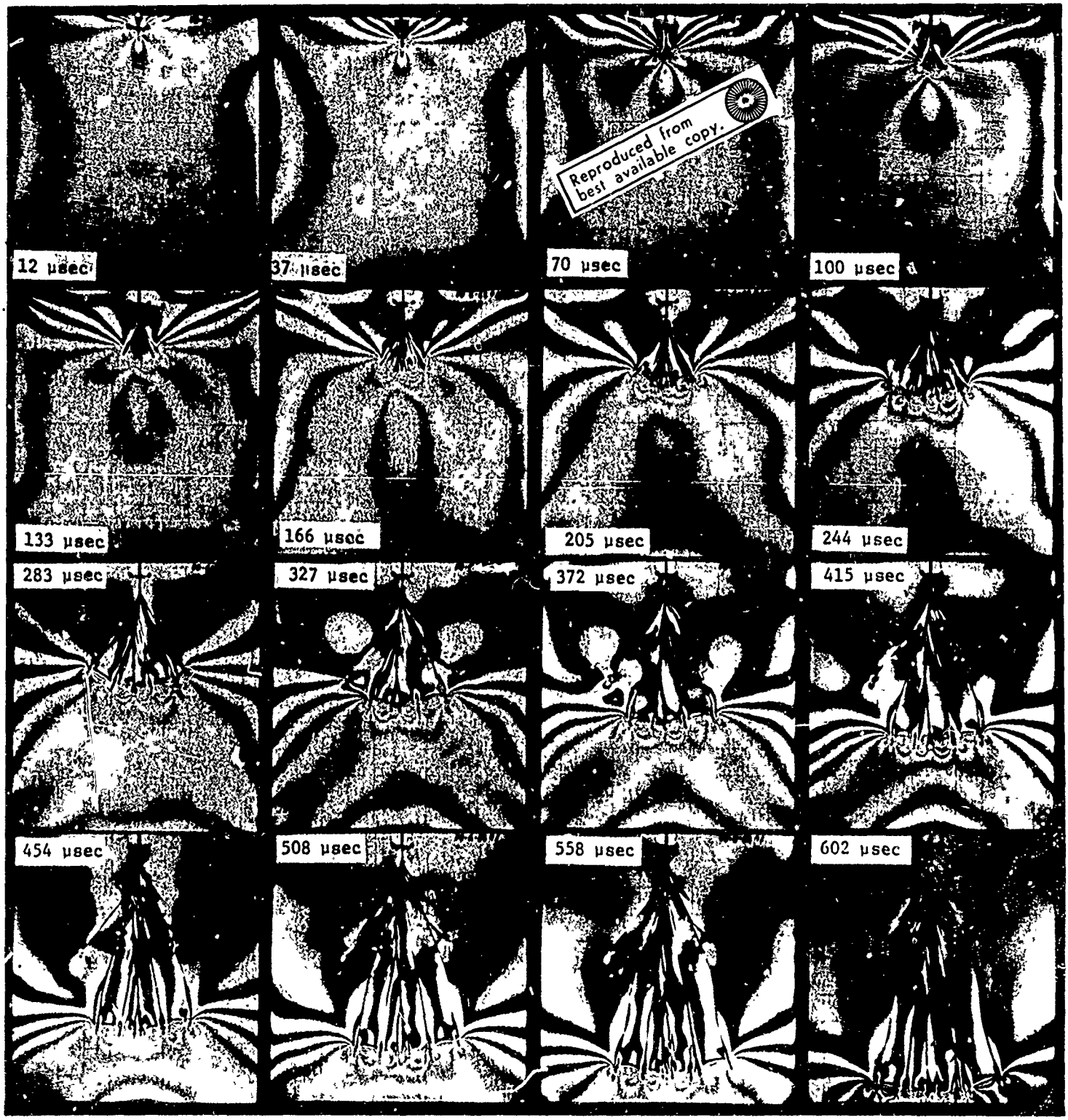

Figure 5. Isochromatic Patterns of Dynamic Crack Propagation for Test No. 5

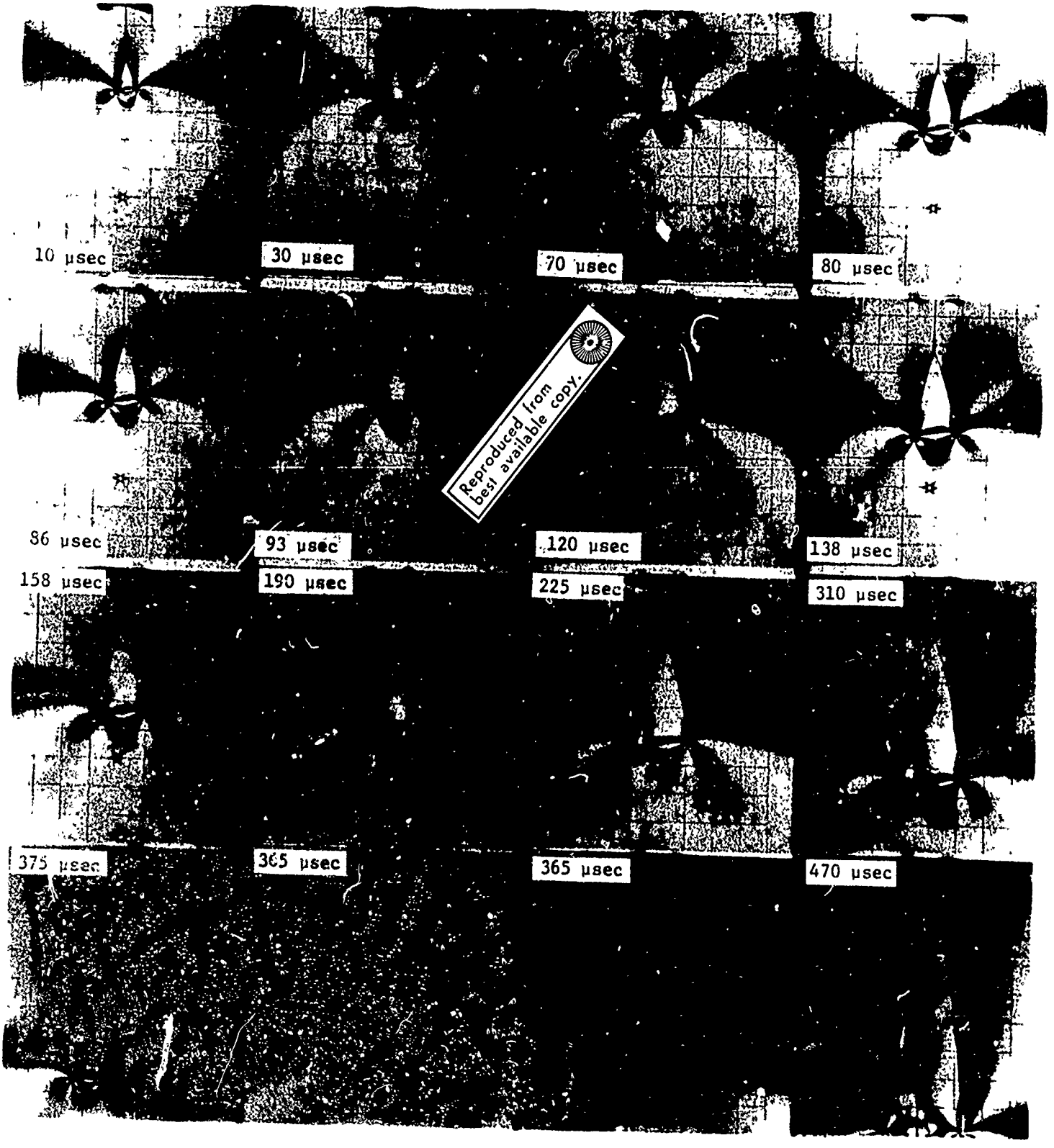

Figure 6. Isochromatic Patterns of Dynamic Crack Propagation for Test No. 7

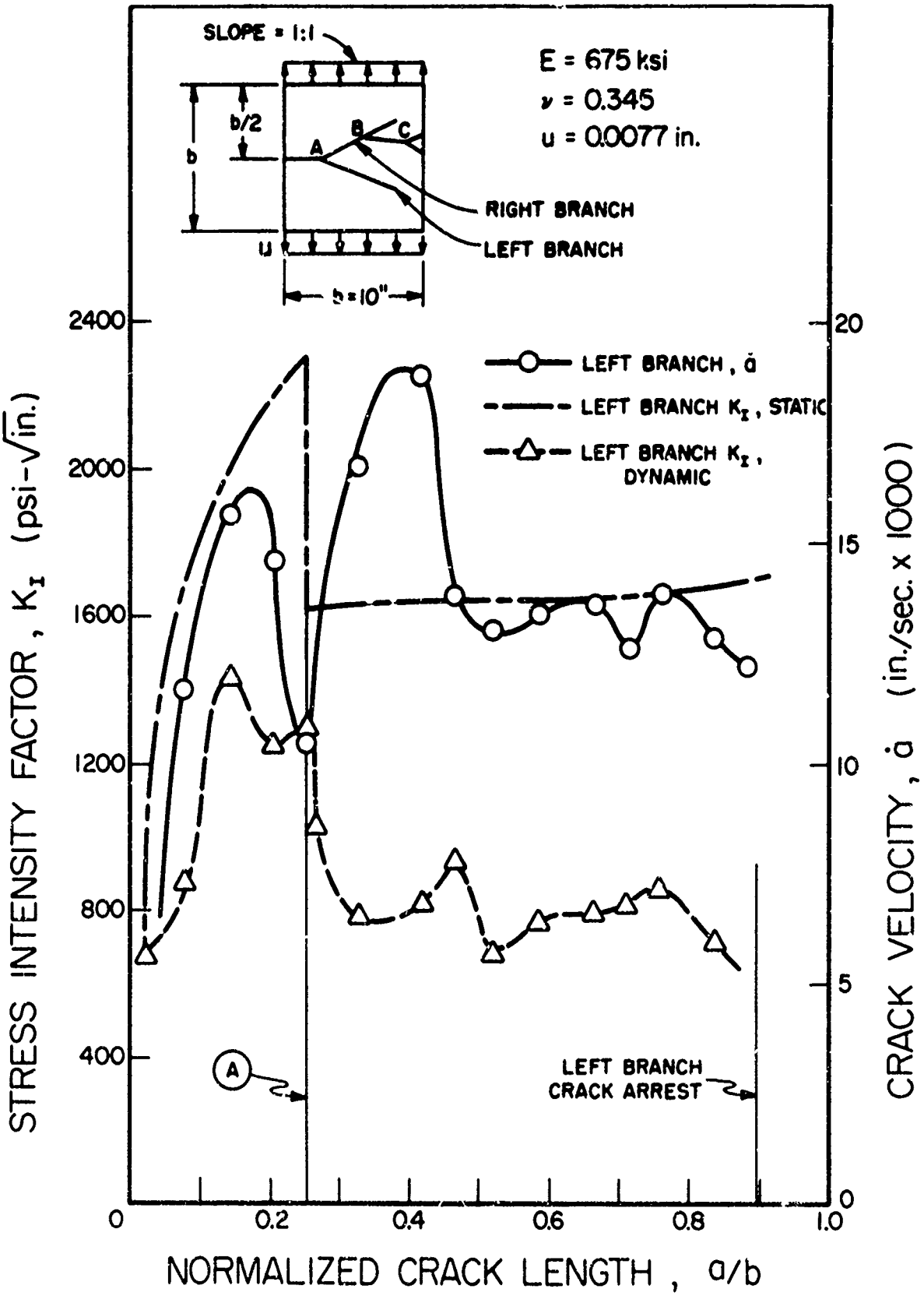

FIGURE 7a. STRESS INTENSITY FACTORS & CRACK VELOCITIES IN A SINGLE EDGE NOTCHED PLATE SUBJECTED TO A UNIFORM EDGE DISPLACEMENT , TEST NO. 3 . LEFT BRANCH

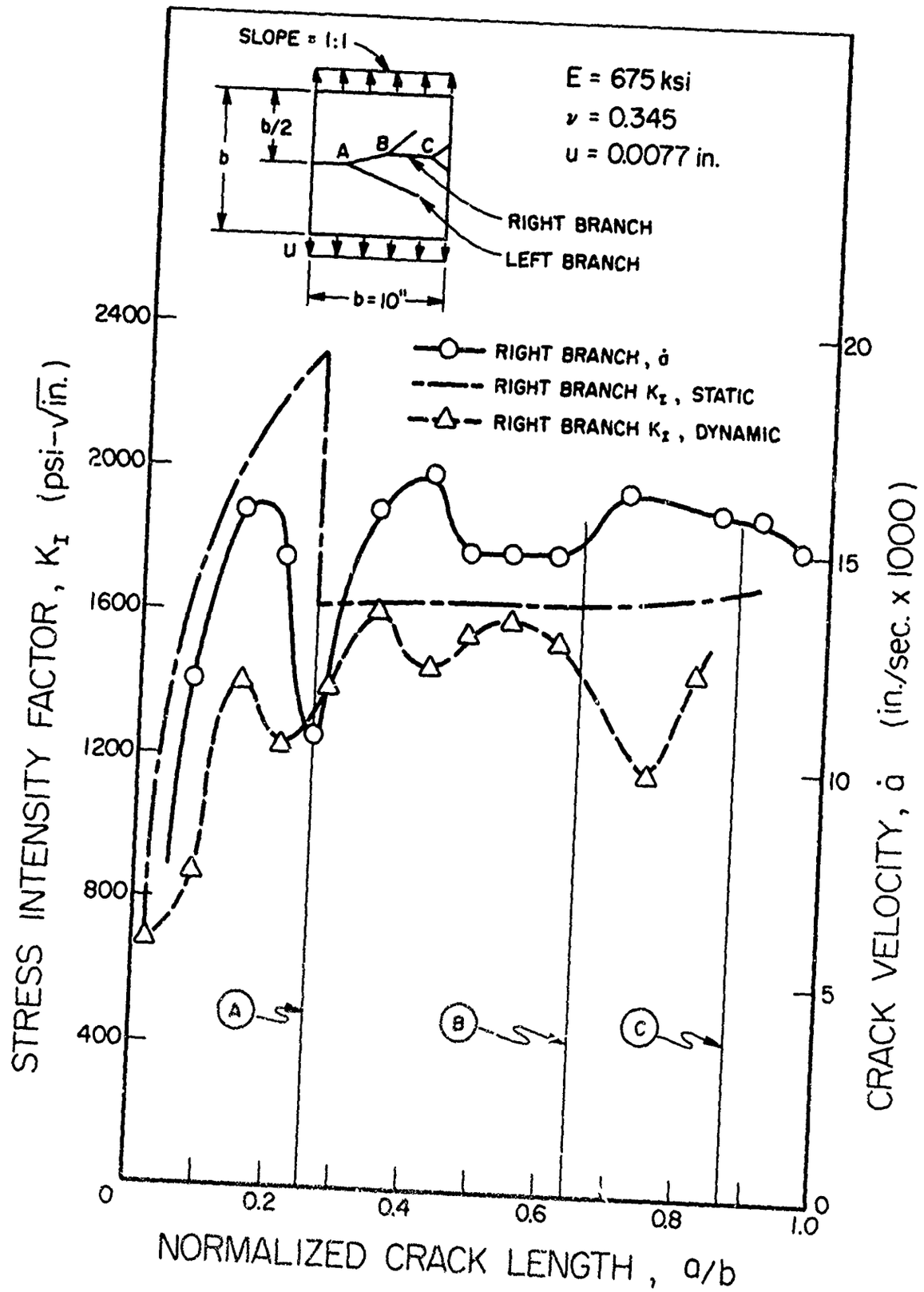

FIGURE 7b. STRESS INTENSITY FACTORS & CRACK VELOCITIES IN A SINGLE EDGE NOTCHED PLATE SUBJECTED TO A UNIFORM EDGE DISPLACEMENT, TEST NO. 3. RIGHT BRANCH

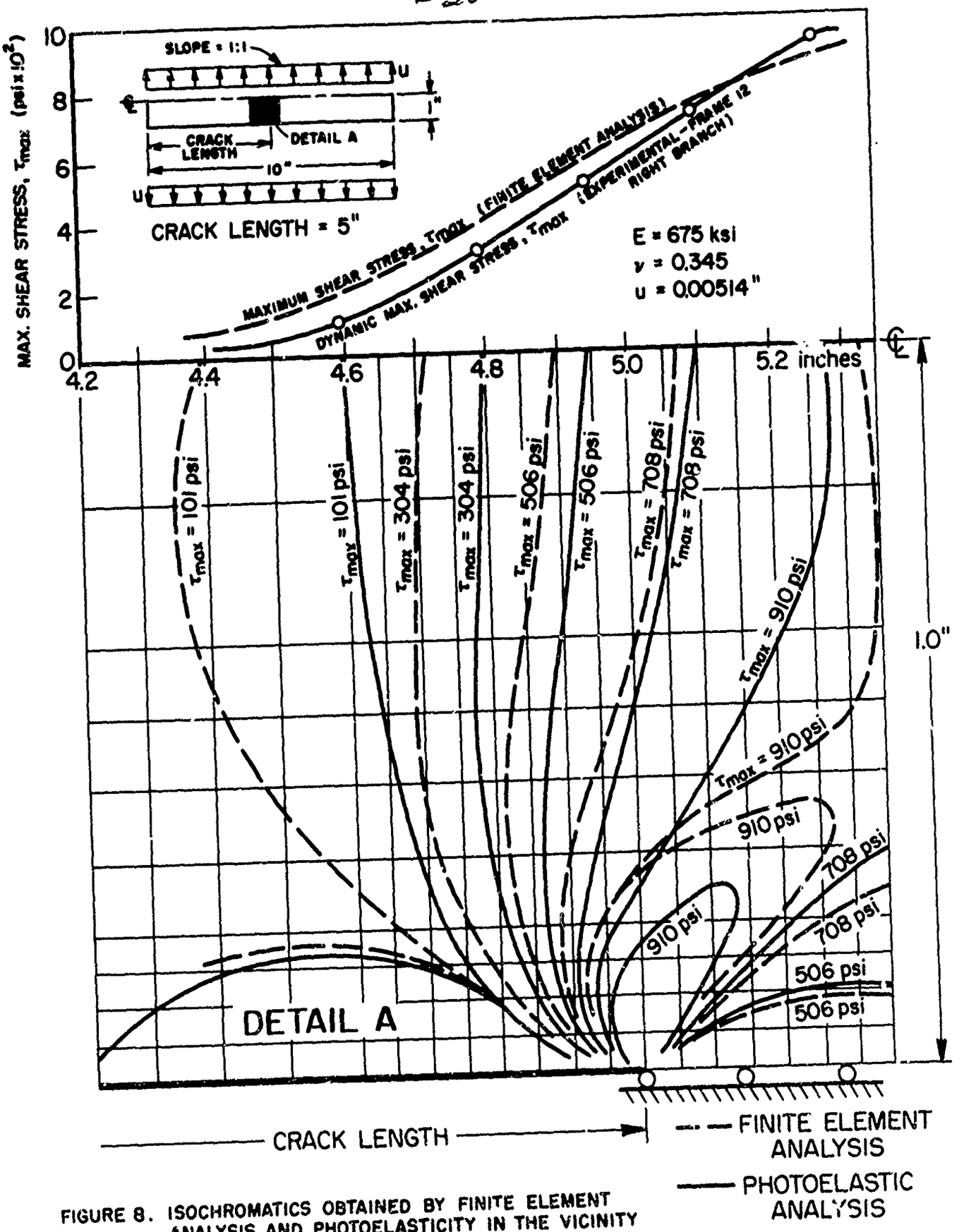

FIGURE 8. ISOCHROMATICS OBTAINED BY FINITE ELEMENT ANALYSIS AND PHOTOELASTICITY IN THE VICINITY OF A CRACK TIP OF A MULTIPLY BRANCHED CRACK.

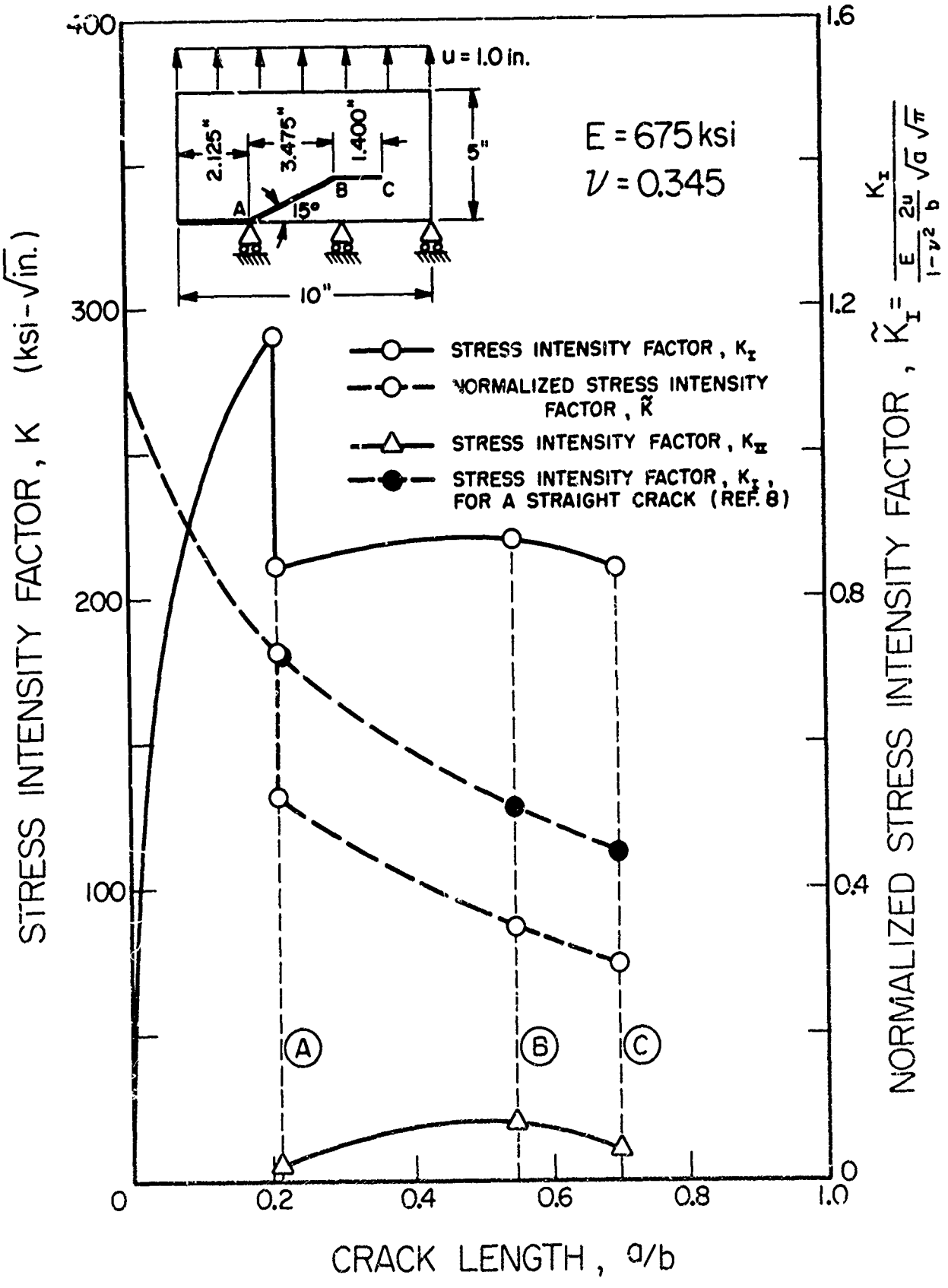

FIGURE 9. STATIC STRESS INTENSITY FACTOR FOR A BRANCHED CRACK IN AN EDGE CRACKED PLATE SUBJECTED TO UNIFORM EDGE DISPLACEMENT LOADING.

FIGURE 10. FRACTURE SURFACE OF LEFT AND RIGHT BRANCH CRACKS OF TEST NO. 3.

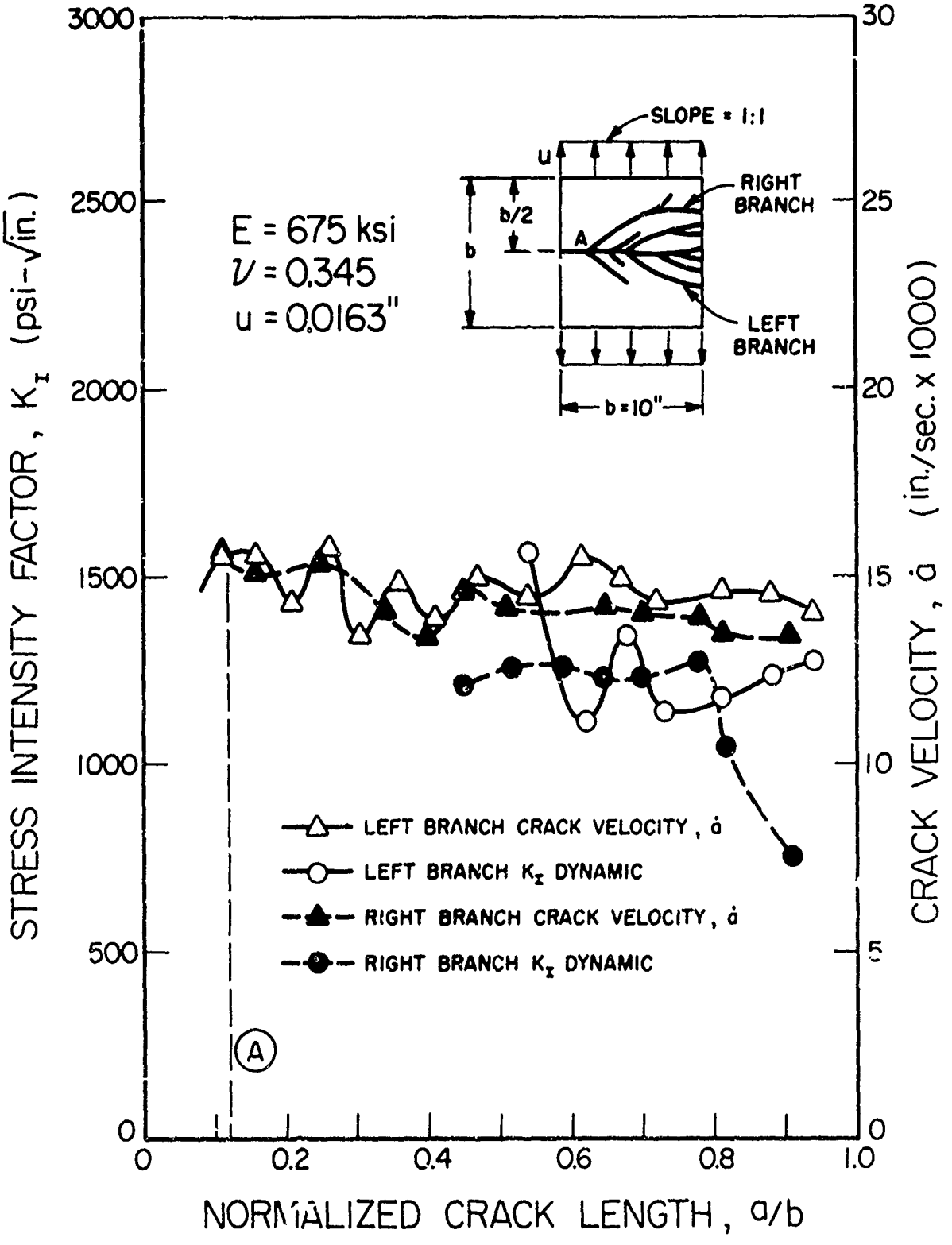

FIGURE 11. STRESS INTENSITY FACTORS & CRACK VELOCITIES IN A SINGLE EDGE NOTCHED PLATE SUBJECTED TO A UNIFORM EDGE DISPLACEMENT, TEST NO. 5

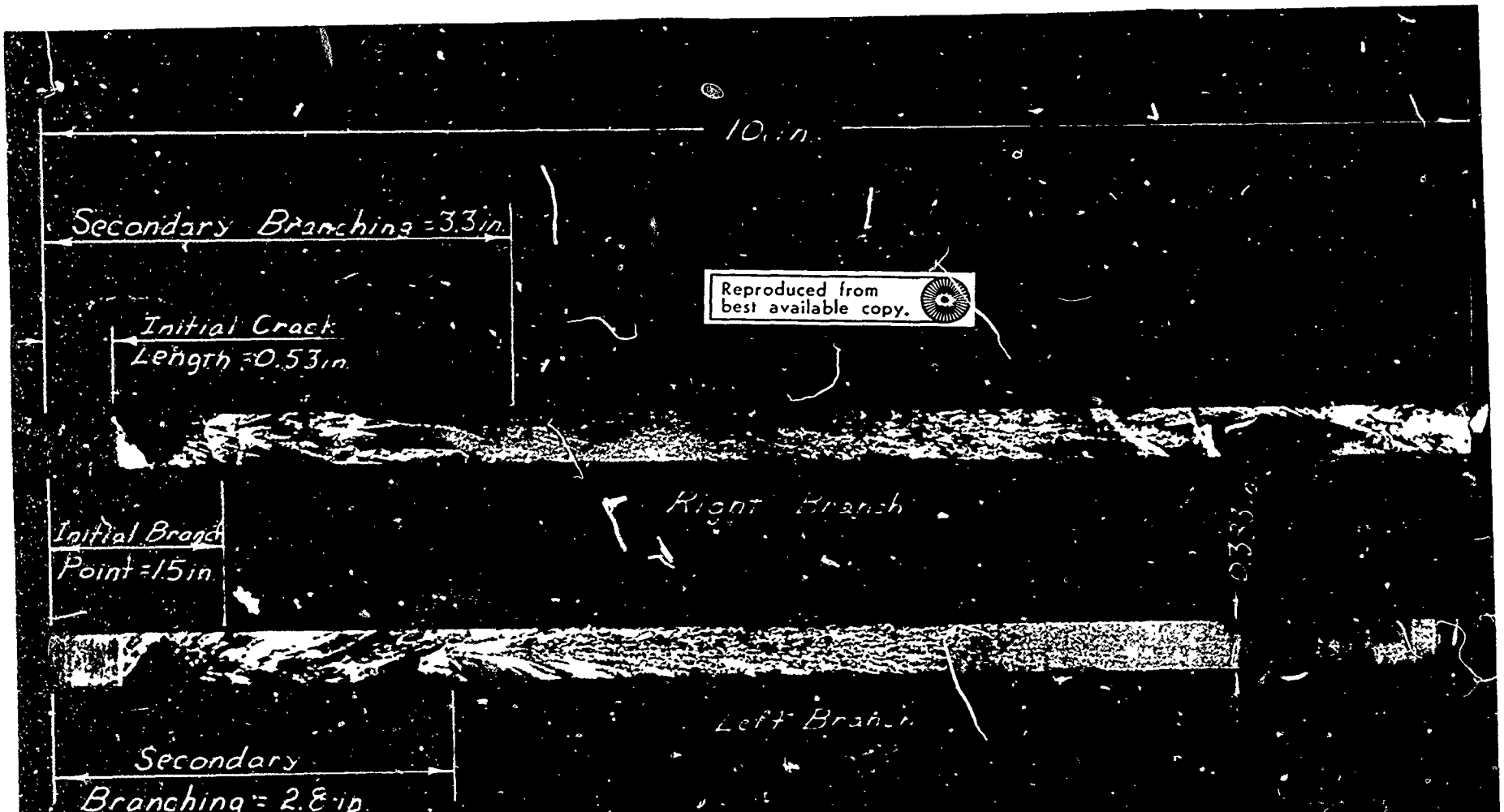

FIGURE 12. FRACTURE SURFACE OF LEFT AND RIGHT BRANCH CRACKS OF TEST NO. 5.

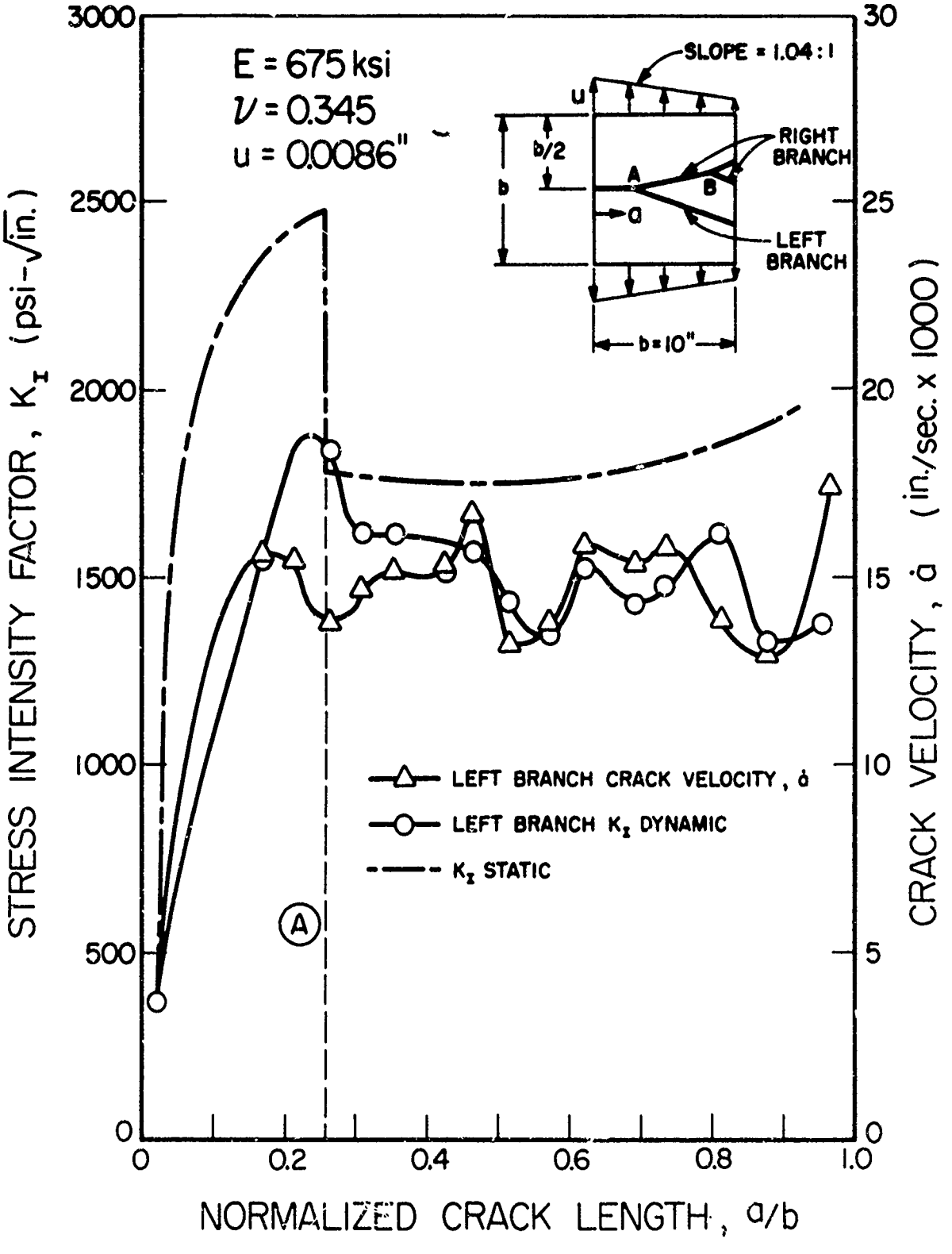

FIGURE 13a. STRESS INTENSITY FACTORS & CRACK VELOCITIES IN A SINGLE EDGE NOTCHED PLATE SUBJECTED TO VARIABLE EDGE DISPLACEMENTS, TEST NO. 1 LEFT BRANCH

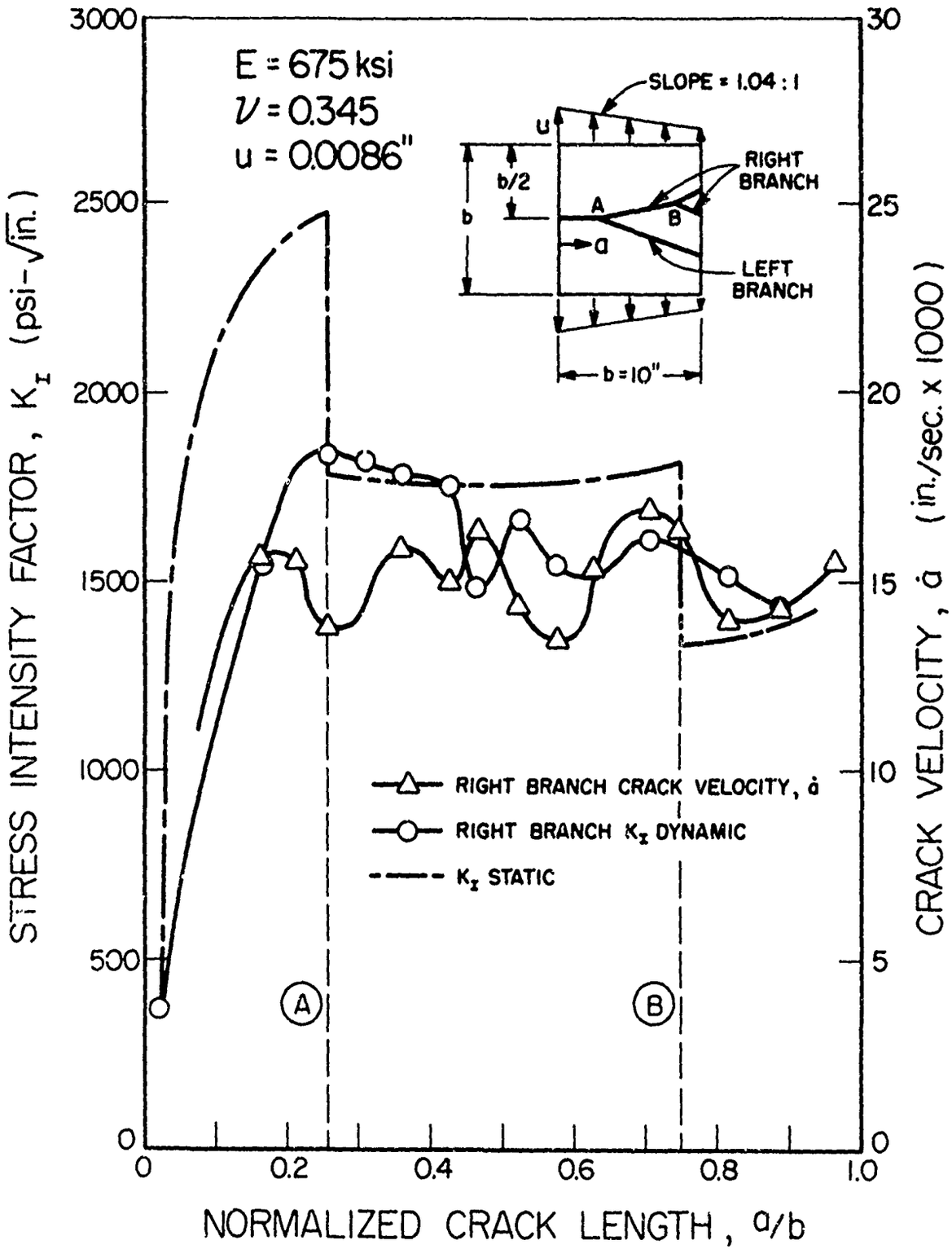

FIGURE 13b. STRESS INTENSITY FACTORS & CRACK VELOCITIES IN A SINGLE EDGE NOTCHED PLATE SUBJECTED TO VARIABLE EDGE DISPLACEMENTS, TEST NO. 1 RIGHT BRANCH

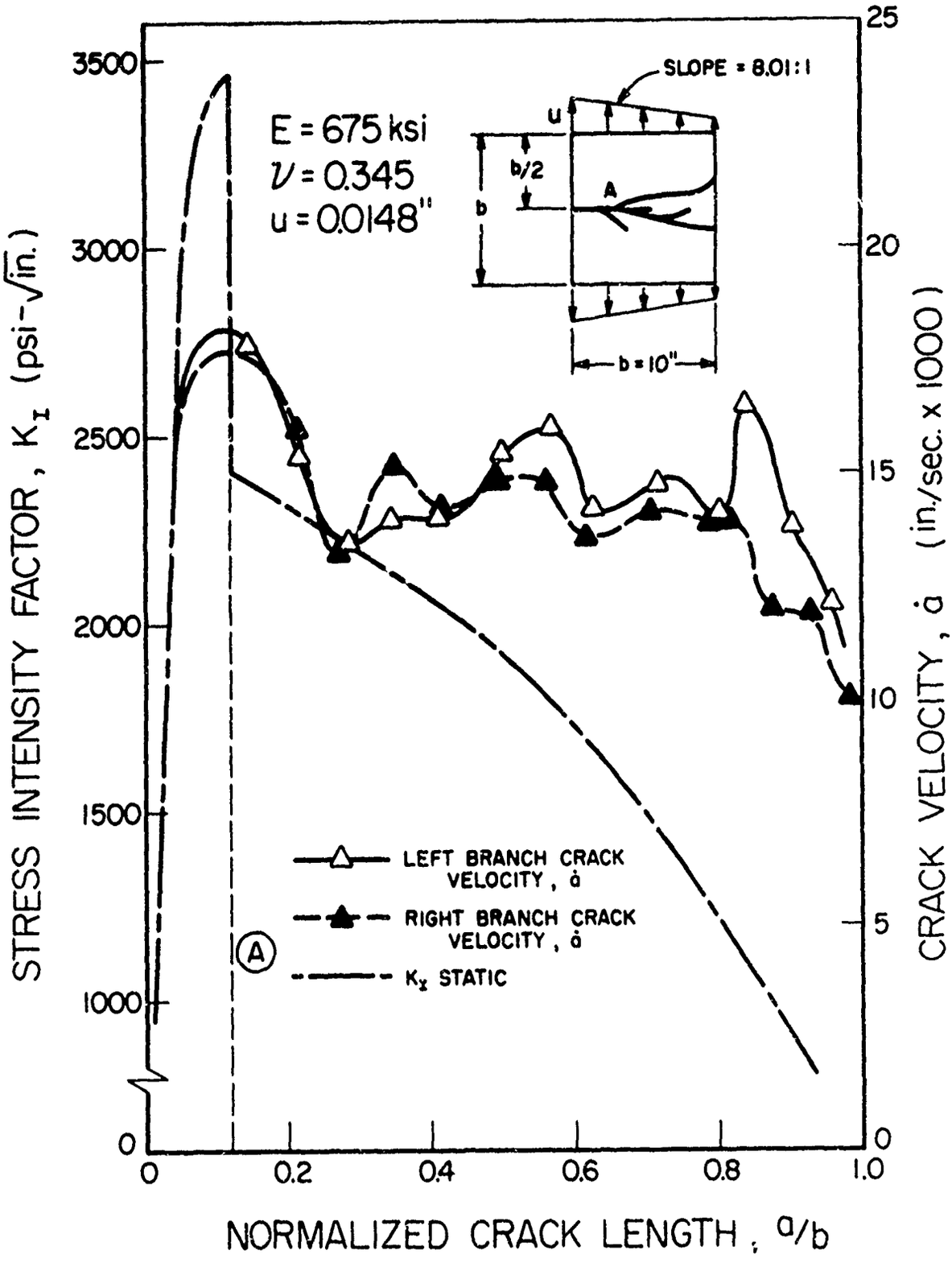

FIGURE 14. STRESS INTENSITY FACTORS & CRACK VELOCITIES IN A SINGLE EDGE NOTCHED PLATE SUBJECTED TO A VARIABLE EDGE DISPLACEMENT, BRADLEY TEST NO. 2

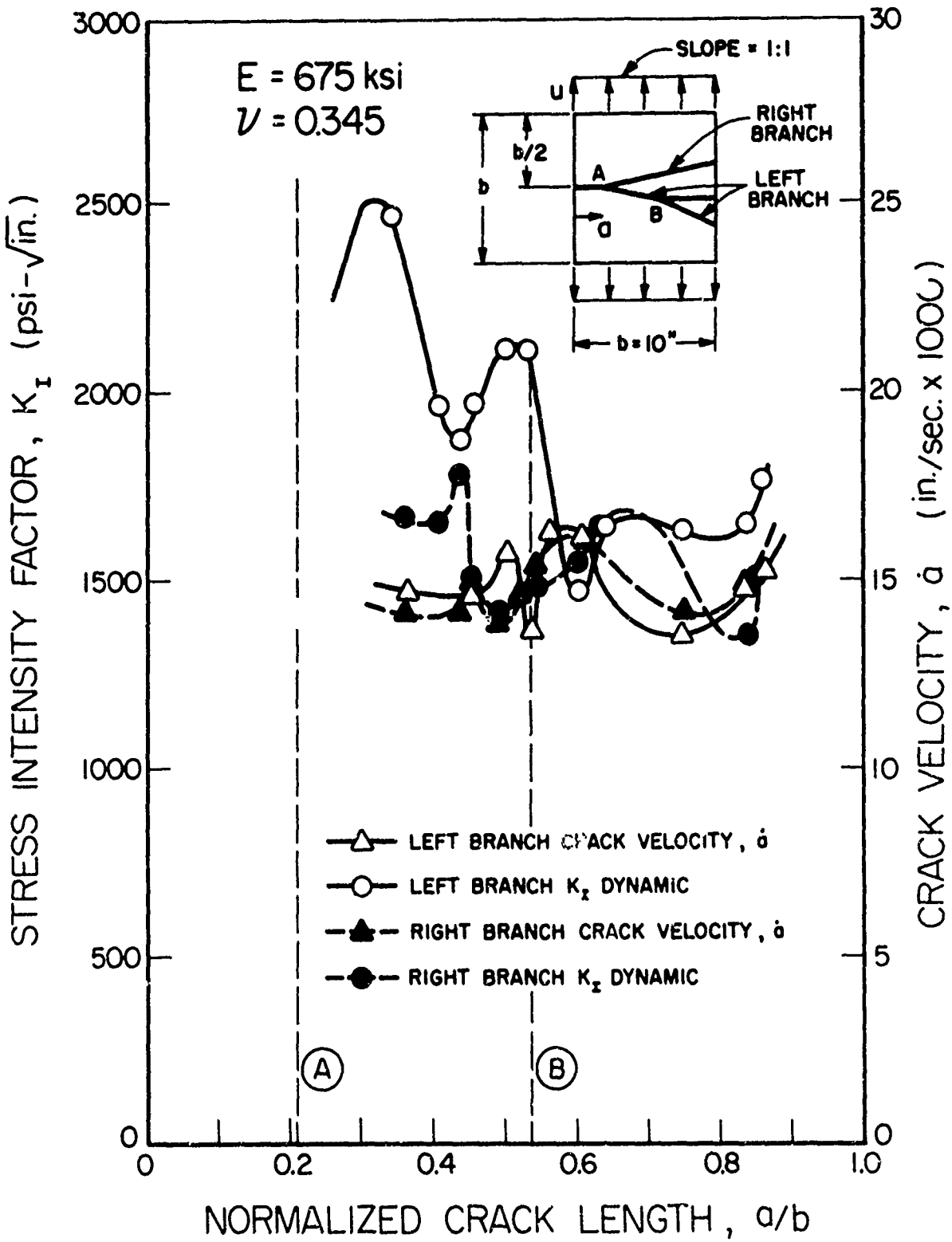

FIGURE 15. STRESS INTENSITY FACTORS & CRACK VELOCITIES IN A SINGLE EDGE NOTCHED PLATE SUBJECTED TO A UNIFORM EDGE DISPLACEMENT, TEST NO. 7

FIGURE 16. ENLARGED PHOTOGRAPH OF FRAME 11 OF TEST NO. 5.